Effects of Annealing Temperature on Magnetic Property and Structure of Amorphous $Co_{49}Pt_{51}$ Alloy Nanowire Arrays Prepared by Direct-Current Electrodeposition

Hua Li, Cai-Ling Xu, Guang-Yu Zhao, and Hu-Lin Li*

College of Chemistry and Chemical Engineering, Lanzhou University, Lanzhou 730000, P.R. China

Received: October 12, 2004

$Co_{49}Pt_{51}$ nanowire arrays with an average diameter of 35 nm and lengths up to several micrometers were grown in an ordered porous anodic aluminum oxide (AAO) template using direct-current electrodeposition. The as-deposited samples were annealed at 100, 200, 300, 400, 500, 600, and 700 °C, respectively. The temperature dependence of the magnetic property of the $Co_{49}Pt_{51}$ nanowire arrays associated with the microstructure was analyzed by X-ray diffraction and a vibrating sample magnetometer. Magnetic measurements show that the samples both as-prepared and annealed at low temperatures have excellent perpendicular anisotropy. The perpendicular coercivity ($H_{c\perp}$) of $Co_{49}Pt_{51}$ alloy nanowire arrays increases dramatically as the annealing temperature (T_A) rises, reaches a maximum($H_{c\perp}$ = 2770 Oe) at 400 °C, and then decreases sharply as T_A rises further. This phenomenon should be attributed to the special structure of the nanowire arrays/AAO, and the microstructure factors significantly change during the annealing process.

1. Introduction

Magnetic nanowires, fabricated by various methods, have recently attracted much attention because of their potential application in ultra-high-density magnetic recording media.[1,2] Nanoscale patterned arrays have been suggested as recording media to achieve recording densities of more than 100 Gbit/in^2.[3,4] This storage density is much higher than that of current commercial hard disks (3.7 Gbit/in^2) and also beyond the projected thermal limit of 40 Gbit/in^2 in continuous magnetic film.[5] One promising technique with which to obtain nanomagnet arrays is based on the template method.[6] Compared with other templates, the hole size of anodic aluminum oxide (AAO) can be readily controlled by properly adjusting the anodizing condition. The AAO template is also thermally stable and shows hexagonally ordered porous structures with nanochannel density in the range $10^{11}-10^{13}$/cm^2.[7]A unit cell of magnetic nanowire arrays acts as a recording cell.[8] These merits make it an ideal template for preparing magnetic nanowire arrays. The general procedure to produce arrays of nanowires is electrochemical deposition, which also allows the production of multilayers.

In our previous work, we had successfully prepared magnetic nanowire arrays filled in a porous AAO template, such as Fe, Co, CoNi, Fe_xCo_{1-x}, and CoPt/Pt nanowires.[9−14] Other research groups also reported the successful preparation of metal nanowire arrays such as Ni,[15] FeNi,[16] Co/Cu,[17] Ni/Cu,[18] NiFe/Cu,[19] CoNi/Cu,[20] and Ag/Co[21]nanowires. Although there have been numerous publications about heterogeneous ferromagnetic−nonmagnetic alloy nanowire arrays such as CoPd,[22] CoCu,[23] CoPb,[24] CoAg,[25] and FeAg[25] grown by AAO template, Co−Pt alloy nanowire array systems have been scarcely reported in the literature, and furthermore, most of the work on 1D magnetic nanomaterials have mainly focused on the polycrystalline structure alloy. To the best of our knowledge, the effects of different annealing temperatures on magnetic properties and microstructure of amorphous Co−Pt alloy nanowire arrays have not been reported so far. In this paper, an interesting amorphous magnetic Co−Pt alloy nanowire array has been successfully fabricated by direct current (dc) electrodeposition in a porous AAO template. Magnetic measurements demonstrated that the as-prepared material has good magnetic properties, and both the perpendicular coercivity and squareness of the samples annealed at or below 400 °C have been enhanced, but the excellent magnetic properties disappeared rapidly as the annealing temperature was further increased. The temperature dependence of the magnetic property of the $Co_{49}Pt_{51}$ nanowire arrays associated with the microstructure is discussed in detail.

2. Experimental Section

2.1. Fabrication and Annealing. The ordered porous alumina membranes were prepared via a two-step anodizing process described in detail in our previous work.[14] The as-prepared template was dipped into 5% phosphoric acid at 50 °C for 25 min to eliminate the obstacle film, and then, a silver film of 300-nm thickness was sputtered onto one side of the template to act as a conductive contact.

Electrodeposition was carried out at room temperature, using a three-electrode potentiostatic control and a dc electrodeposition system with a saturated calomel electrode (SCE) as the reference electrode, a 1 cm × 0.5 cm platinum plate as a counter electrode and the Ag-coated AAO template as the working electrode. The magnetic component is present at 49 at. %. To achieve this composition in electrodeposited $Co_{49}Pt_{51}$ alloy nanowires, the relative Co concentration has to be greatly increased owing to the extremely high rate of Pt deposition compared to that of Co. The $Co_{49}Pt_{51}$ alloy nanowires used in the experiments described here were grown from a solution of 1.5 mol·dm^{-3} of $CoSO_4 \cdot 7H_2O$, 0.012 mol·dm^{-3} of H_2PtCl_6 , and 40 g·dm^{-3} of boric acid, at 1.0 V (vs SCE). Definitely, on the basis of these values, the component of Co_xPt_{1-x} alloy nanowires can be easily controlled by adjusting the relative concentration of Co^{2+} and Pt^{4+} in the electrolyte. The pH value of the solution was 3.0, adjusted with H_2SO_4. In deposition experiments, the solution was unstirred. To study the annealing effects on $Co_{49}Pt_{51}$ alloy

* Corresponding author. Phone: +86-931-891-2517. Fax: +86-931-891-2582. E-mail address: lihl@lzu.edu.cn.

10.1021/jp045347t CCC: $30.25
Published on Web 02/15/2005

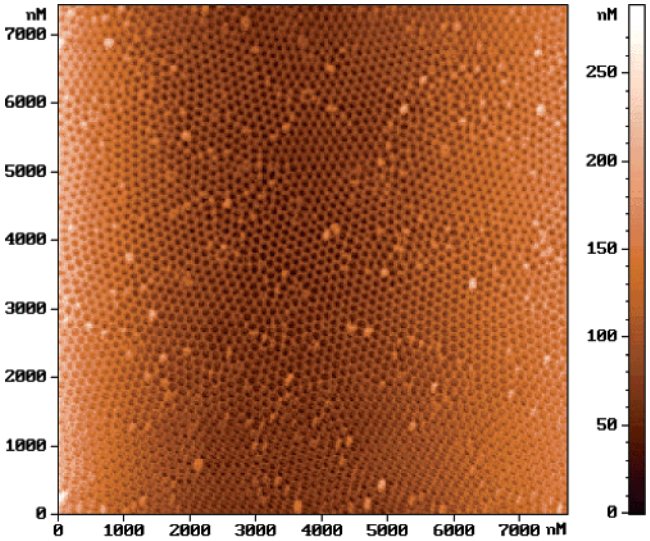

Figure 1. AFM image of the surface of an AAO template after the second anodization.

nanowire arrays, all samples were annealed for 1 h at different temperatures (100, 200, 300, 400, 500, 600, and 700 °C) in an Ar (99.999%) atmosphere.

2.2. Sample Preparation for SEM and TEM Observations. To obtain the scanning electron microscopy (SEM) image of the $Co_{49}Pt_{51}$ nanowire arrays, the sample was dipped into a solution of 6% H_3PO_4 and 1.8% H_2CrO_4 at 50 °C for 30 min to erode the upper part of the AAO. For transmission electron microscopy (TEM) imaging, we dipped the as-prepared samples into 6% H_3PO_4 and 1.8% H_2CrO_4 at 50 °C for 180 min to dissolve the AAO completely.

2.3. Characterization. The morphology of the AAO templates was examined by atomic force microscopy (AFM, P47-SPM). TEM (Hitachi 600) and SEM (JEOL JSM-5600LV) were used to characterize the morphology of the nanowire arrays. The crystalloid structure of the samples was determined by X-ray diffraction (XRD, Rigaku, model D/max 2400; Cu Kα radiation, $\lambda = 1.54056$ Å). The average composition of the nanowires was measured from energy dispersive spectra (EDS, JEOL JSM-5600LV). Magnetic properties of the as-prepared and annealed samples were tested by a vibrating sample magnetometer (VSM, TOEI-5S-15).

3. Results and Discussion

Figure 1 shows a typical AFM micrograph of the AAO template. One can see that the anodic alumina template has almost arranged the pore array with the average diameter of the pores about 35 nm and the interpore distance about 60 nm. The pore density is about 10^{11} cm^{-2}. The diameter and interval of the pores are based on the applied voltage. AAO membranes with different pore diameters and depths can be prepared by adjusting the applied voltage and using different electrolytes. Generally, the higher the anodized voltage is, the larger the pore diameter of AAO film is; the longer the time is, the thicker the film is and the deeper the pores are.

Figure 2 shows the morphology images of the as-grown $Co_{49}Pt_{51}$ nanowire arrays that are acquired by SEM. Figure 2a is a top view image, and Figure 2b is a closeup view image of Figure 2a. From Figure 2, we can find several clusters of nanowires. The clusters could result from the situation in which the nanowires are uncovered from the framework of the AAO template but free-standing incompletely. When the top alumina of the AAO template was dissolved away, the nanowires

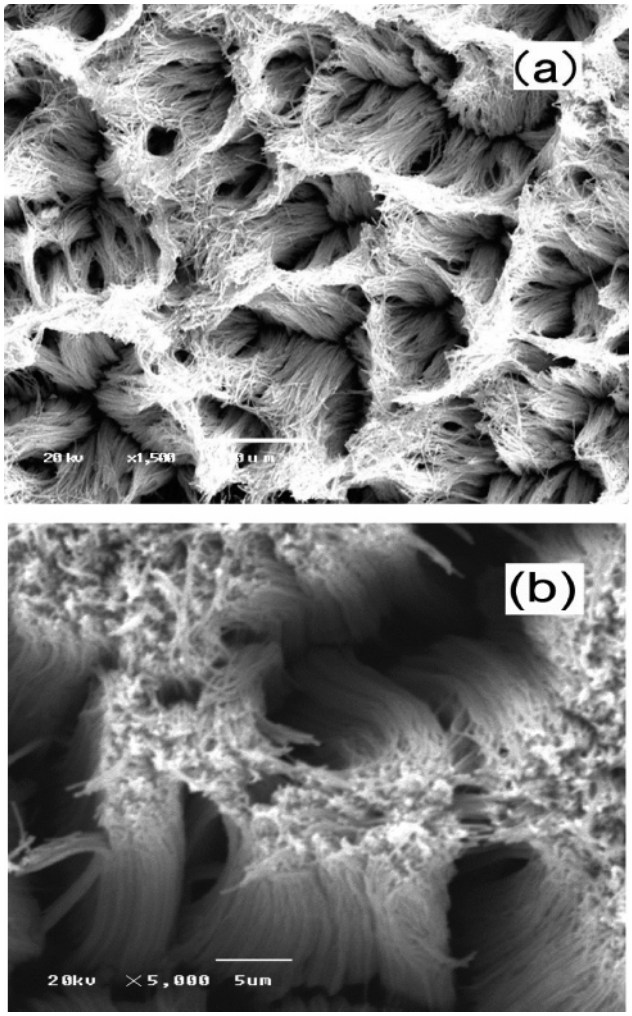

Figure 2. SEM micrographs of uniform $Co_{49}Pt_{51}$ nanowire arrays fabricated by electrodeposition: (a) the view from the top, and (b) the closeup view of (a).

embedded in the template were released gradually and inclined to agglutinate together. It is conceivable that the surface energy of the nanowires causes this interesting phenomenon. Figure 2 also shows that the $Co_{49}Pt_{51}$ nanowires are abundant, uniform, and well-ordered in the large area. From the figures, it can be estimated that the length of the $Co_{49}Pt_{51}$ nanowires is more then 10 μm, corresponding to the thickness of the AAO template used and the high pore filling rate (about 90%).

The as-prepared $Co_{49}Pt_{51}$ nanowires were characterized by TEM after the AAO template had been completely dissolved. TEM images (Figure 3a,b) reveal that the $Co_{49}Pt_{51}$ nanowires fabricated by the AAO template method are of regular size and are continuous. All of them have a uniform diameter of about 35 nm, which basically equals that of the pores of the AAO template used in the experiment. However, in the TEM picture, nanowires show different contrasts within themselves. This can be explained by the formation of nanowires by small particles with different compositions and atomic weights. In this case, the electron-dispersing ability of Co particles is stronger than that of Pt particles, and hence, the darker sections correspond to Pt while the brighter sections correspond to Co. The average length of $Co_{49}Pt_{51}$ nanowires prepared by electrodeposition for 1 h is above 10 μm, and the typical diameter is about 35 nm (i.e., the aspect ratio is 300 or greater).

To confirm the chemical concentration of the as-grown nanowires, EDS at the same position as in Figure 2a was

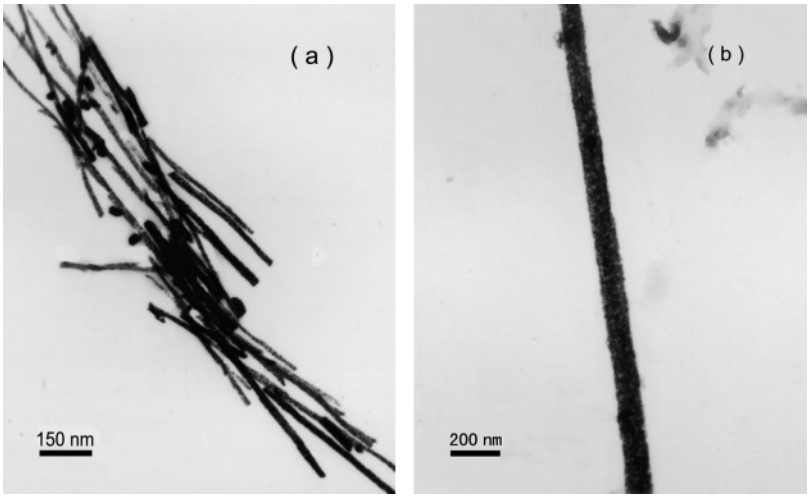

Figure 3. TEM images of (a) several $Co_{49}Pt_{51}$ nanowires, (b) a single $Co_{49}Pt_{51}$ nanowire with diameter of 35 nm.

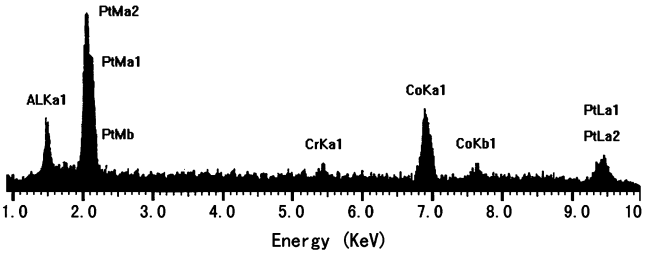

Figure 4. EDS pattern of the Co−Pt alloy nanowires. The composition ratio of the nanowires was 48.85 at. % Co, 51.15 at. % Pt.

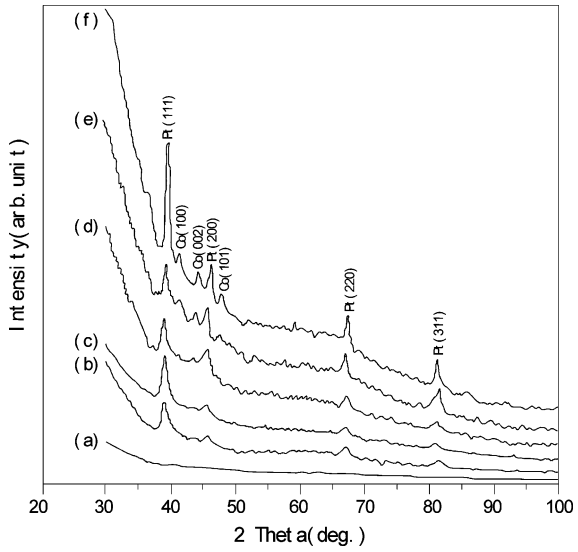

Figure 5. XRD patterns of electrodeposited $Co_{49}Pt_{51}$ alloy nanowire arrays at (a) room temperature and after annealing for 1 h at various temperatures T_A's: (b) 300, (c) 400, (d) 500, (e) 600, and (f) 700 °C.

measured. This EDS analysis demonstrates that the quantitative atomic ratio of Co to Pt in the corresponding nanowires is close to 49:51 (Figure 4). The EDS pattern also shows the peaks of elements Cr and Al, which are attributed to the remaining H_2CrO_4 from the acid etching and the AAO template, respectively.

The typical XRD patterns of $Co_{49}Pt_{51}$ nanowire arrays with different annealing temperatures are shown in Figure 5. The XRD measurement shows that no obvious reflection peak in Figure 5a was found, indicating amorphous-like structure of the as-deposited material. Whether the deposit is amorphous or crystalline depends on the growth conditions such as applied voltage, electrolyte concentration, and so on.[26] We know that, under equilibrium conditions, the mutual solubility of ferromagnetic and nonmagnetic metal is very low in both the solid and liquid forms, such as Co and Cu, Co and Ag, and Co and Pt. However, under nonequilibrium conditions, such systems could form metastable phases.[24,25] In this type of material, the annealing treatment results in the recrystallization of this metastable alloy into two separate phases, leading to the formation of small ferromagnetic metal particles that exhibit greatly enhanced magnetic properties because of their single-domain nature.[27] These processes have already been proven by XRD and are shown in Figure 5. The XRD measurement shows that all peaks ((111), (200), (220), and (311)) of our sample annealed below 500 °C are consistent with those of a typical face-centered-cubic (fcc) Pt structure. The peak positions and their relative intensities are consistent with the standard power diffraction pattern of fcc Pt. Neither fcc nor hexagonal-close-packed (hcp) Co peaks are detected from the XRD spectra of the samples annealed below 500 °C. It is believed that the Co−Pt alloy nanowires are in a metastable phase below 500 °C because of the quick rate of electrodeposition under nonequilibrium conditions. Further annealing at 500 °C or above reveals a well-developed hcp Co phase with the peaks of (100), (002), and (101) (Figure 5e,f), suggesting a phase separation in this alloy system. This is similar to the Fe−Ag alloy, the Co−Ag alloy, and the Co−Cu alloy.[25,28] As T_A was increased to or above 600 °C, the diffraction lines became progressively narrower because of the growth of particle size. It is generally recognized that the AAO is amorphous or nanocrystalline with a mean crystallite size of less than 4 nm.[29] The XRD patterns show that the AAO remained amorphous when the annealing temperature was equal to or lower than 700 °C for 1 h. It is consistent with the research of Sui et al.[30]

The effects of annealing temperature (T_A) on the coercivity and squareness of $Co_{49}Pt_{51}$ alloy nanowires embedded in AAO measured at room temperature is shown in Figure 6a,b. At first, we note that the coercivity ($H_{c\perp}$) and squareness ($M_r/M_{s\perp}$) measured with the external field applied perpendicular to the sample surface are always larger than those of the parallel external field, because of the preferential orientation of the nanowires.[31] As the annealing temperature increases from 100 to 300 °C, the perpendicular coercivity has a weak increase. However, we found that the perpendicular coercivity increases dramatically with the annealing temperature up to 400 °C, reaches its maximum (2770 Oe), and then decreases as T_A is increased further. From Figure 6a, we can also see that, with

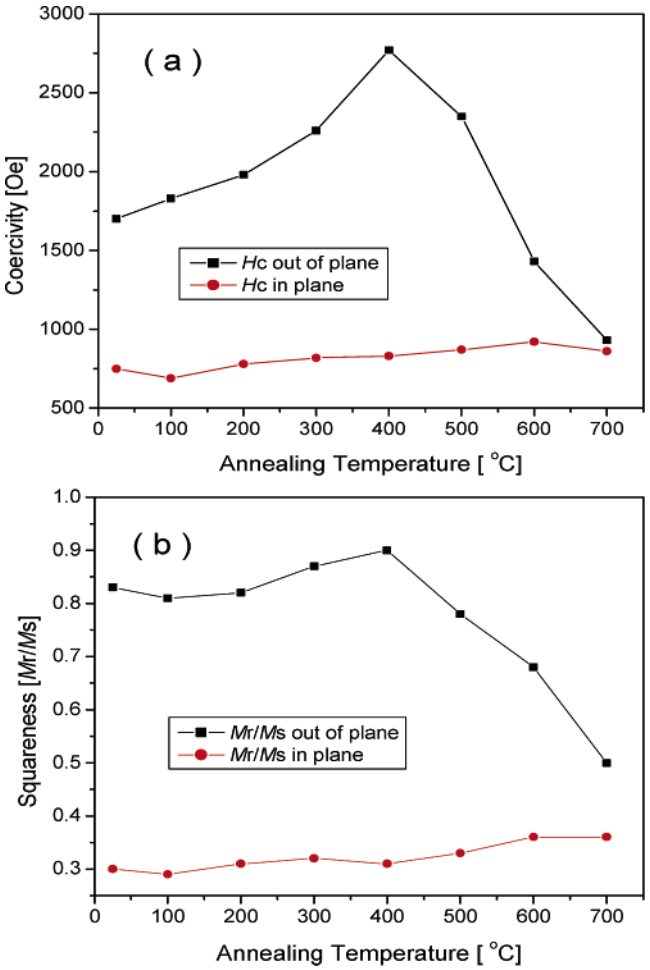

Figure 6. Coercivity (a) and squareness (b) as functions of temperature. (Out-of-plane means the applied field is parallel to the nanowires; in-plane means the field is perpendicular to the nanowires.)

the increase of annealing temperature, the obvious change has not been observed in $H_{c\|}$, which is much different from that in the ferromagnetic−nonmagnetic alloy films.[32] This can be attributed to the structural difference between the films and the nanowires. The ordered nanowires with high aspect ratios (length to diameter, greater than 300) in AAO are separated from each other; namely, the nanowires have highly anisotropic structure. This structure induces the $Co_{49}Pt_{51}$ alloy to tend to expand along the wire axis during annealing and form a column structure with an easy axis along the nanowire arrays, which will improve shape anisotropy at the local region. Figure 6b shows the squareness (M_r/M_s) measured at room temperature as a function of annealing temperature for $Co_{49}Pt_{51}$ alloy nanowires embedded in AAO. Figure 6b indicates that, as T_A rises, an increase in the perpendicular squareness of $Co_{49}Pt_{51}$ alloy nanowire arrays is seen and the maximum perpendicular squareness $M_r/M_{s\perp} = 0.9$ at $T_A = 400$ °C. And then, the value of the perpendicular squareness decreases rapidly as the annealing temperature is further increased. However, squareness is always less than 0.4 when the applied field is perpendicular to the nanowires. Studies of squareness indicate that both the as-prepared samples and the samples annealed at low temperatures (≤400 °C) have excellent perpendicular anisotropy with the easy axis parallel to the nanowires. We propose that the change of magnetic properties of $Co_{49}Pt_{51}$ alloy nanowire arrays after annealing is related to a microstructure change during the annealing process. Because of the rapid dc electrodeposition of Co^{2+} and Pt^{4+} into the AAO template, intrinsic stress and defects are high. As the annealing temperature increases from 100 to 400 °C, the coercivity and squareness increase due to structural relaxation and reduction of defects. Furthermore, there is a large mismatch between the thermal expansion coefficients (α) of $Co_{49}Pt_{51}$ alloy and alumina. The α value (about 11.0×10^{-6} K^{-1}) of Co−Pt alloy is much higher than that of AAO (about 6.0×10^{-6} K^{-1}). That is to say the $Co_{49}Pt_{51}$ alloy tends to expand freely along the wire axis during annealing and form a column structure with its easy axis along the nanowire arrays. So, the shape anisotropy in the local region was improved and led to a great contribution to $H_{c\perp}$, but little to $H_{c\|}$. More column crystals in the local region would make reversal more difficult, which means that high coercivity was obtained. Moreover, the annealing treatment leads to the formation of small Co particles so that the magnetic properties will be improved in the samples. As T_A is increased, the Co grains grow larger in size, leading to the increase of $H_{c\perp}$. This tendency continues until the critical size for these single domain particles is exceeded or when most of the particles begin to coalesce. On the other hand, while annealing at high temperature (above 400 °C), internal stress will increase and the alumina will be distorted. The pore of the AAO template will deviate from its original position, and the shape anisotropy will drop down. In addition, with further annealing at 600 and 700 °C, the hcp Co peaks appeared (see Figure 5e,f). The hcp Co has its easy axis perpendicular to nanowires and decreases anisotropy along nanowire arrays. So, $H_{c\perp}$ in $Co_{49}Pt_{51}$ alloy nanowire arrays drops down in this case. Furthermore, Co will react with O_2 existing in anodic aluminum oxide at high temperature, which deteriorates squareness and decreases perpendicular anisotropy in the alloy arrays.

The highest coercivity we obtained is 2770 Oe in the case of annealing at 400 °C, still much lower than that estimated by the Stoner−Wohlfarth coherent rotation mechanism ($H_c = 2\pi M_s \approx 6400$ Oe).[33] The wire diameter (about 35 nm) is larger than the anisotropy-independent coherence diameter of 7.3 l_{ex}.[34] However, this does not mean that the reversal proceeds by coherent rotation predictions even in the case where the diameter is lower than the coherence diameter, which had been confirmed by Skomski et al.,[35] who proposed that magnetization reversal in very thin nanowires starts by localized nucleation. Because the polycrystallinity state is inhomogeneous, such as the introduction of nanotube and grain misalignment, all these factors will prevent the coherent rotation from occurring in our $Co_{49}Pt_{51}$ nanowire arrays, and a localized reversal mechanism is proposed. Zeng et al.[36] also pointed out that the reversal mechanism should be the localized magnetization reversal model in magnetic nanowire arrays. Certainly, to further understand the reversal mechanism in $Co_{49}Pt_{51}$ nanowires, theory calculations such as the micromagnetic calculation should be carried out, which is not in the scope of this article. The magnetic properties of amorphous Co−Pt alloy nanowire arrays with different diameter and different composition will be reported in our later work.

4. Conclusions

In conclusion, highly ordered amorphous $Co_{49}Pt_{51}$ alloy nanowire arrays were successfully fabricated in the nanochannels of a porous anodic aluminum oxide (AAO) template by direct current electrodeposition. The dependence of structure and magnetic properties of the $Co_{49}Pt_{51}$ alloy nanowire arrays on different annealing temperature were systematically investigated by X-ray diffraction and vibrating sample magnetometer. It is found that the samples both without annealing and annealed at or below 400 °C have perpendicular anisotropy with its easy

axis parallel to the nanowires. Annealing at certain temperatures (≤400 °C) can improve the perpendicular coercivity and squareness in the samples; however, the values of the perpendicular coercivity and squareness decrease rapidly as the annealing temperature is further increased. This phenomenon should be attributed to the special structure of the nanowire arrays/AAO, and the microstructure factors significantly change during the annealing process. The nucleation−propagation localized reversal process is suitable to explain the reversal process in $Co_{49}Pt_{51}$ nanowire arrays.

Acknowledgment. This work is supported by the National Natural Science Foundation of China (NNSFC60471014).

References and Notes

(1) Piraux, L.; George, J. M.; Despres, J. F.; Leroy, C.; Ferain, E.; Legras, R.; Ounadjela, K.; Fert, A. *Appl. Phys. Lett.* **1994**, *65*, 2484.
(2) Blondel, A.; Meir, J. P.; Doudin, B.; Ansermet, J. Ph. *Appl. Phys. Lett.* **1994**, *65*, 3020.
(3) White, R. M.; New, R. M. H.; Pease, R. F. W. *IEEE Trans. Magn.* **1996**, *33*, 990.
(4) Routkevitch, D.; Tager, A. A.; Haruyama, J.; Almawlawi, D.; Moskovits, M.; Xu, J. M. *IEEE Trans. Electron Devices* **1996**, *43*, 1646.
(5) Lu, P. L.; Charap, S. H. *IEEE Trans. Magn.* **1994**, *30*, 4230.
(6) Nielsch, K.; Muller, F.; Li, A. P.; Gosele, U. *Adv. Mater.* **2000**, *12*, 582.
(7) Masuda, H.; Fukuda, K. *Science* **1995**, *268*, 1466.
(8) Daimon, H.; Knakami, O.; Iangoya, O.; Sakemoto, A. *Jpn. J. Appl. Phys*. **1991**, *132*, 282.
(9) Peng, Y.; Zhang, H. L.; Pan, S. L.; Li, H. L. *J. Appl. Phys*. **2000**, *87*, 7405.
(10) Su, Y. K.; Qin, D. H.; Zhang, H. L.; Li, H.; Li, H. L. *Chem. Phys. Lett.* **2004**, *388*, 406.
(11) Qin, D. H.; Peng, Y.; Cao, L.; Li, H. L. *Chem. Phys. Lett.* **2003**, *374*, 661.
(12) Qin, D. H.; Cao, L.; Sun, Q. Y.; Huang, Y.; Li, H. L. *Chem. Phys. Lett.* **2002**, *358*, 484.
(13) Qin, D. H.; Wang, C.W.; Sun, Q.Y.; Li, H, L. *Appl. Phys. A* **2002**, *74(4)*, 761.
(14) Qin, D. H.; Lu, M.; Li, H. L. *Chem. Phys. Lett.* **2001**, *350*, 51.
(15) Paulus, P. M.; Luis, F.; Kroll, M. *J. Magn. Magn. Mater.* **2001**, *224*, 180.
(16) Khan, H. R.; Petrikowski, K. *J. Magn. Magn. Mater.* **2000**, *215*, 526.
(17) Gravier, L.; Wegrowe, J. E.; Wade, T.; Fabian, A.; Ansermet, J. P. *IEEE Trans. Magn.* **2002**, *38*, 2700.
(18) Wang, L.; YuZhang, K.; Metrot, A.; Bonhomme, P.; Troyon, M. *Thin Solid Films* **1996**, *288*, 86.
(19) Dubois, S.; Marchal, C.; Beuken, J. M.; Piraux, L.; Duvail, J. L.; Fert, A.; George, J. M.; Maurice, J. L. *Appl. Phys. Lett.* **1997**, *70*, 396.
(20) Atterborough, K.; Hast, R.; Schwarzacher, W.; Ansermet, J. P.; Blondel, A.; Doudin, B.; Meier, J. P. *Mater. Res. Soc. Symp. Proc.* **1995**, *348*, 3.
(21) Valizadeh, S.; George, J. M.; Leisner, P.; Hultman, L. *Thin Solid Films* **2002**, *402*, 262.
(22) Ding, J. B.; Qin, D. H.; Huang, Y.; Cao, L.; Li, H. L. *J. Mater. Eng. Perform.* **2003**, *12*, 584.
(23) Blythe, H. J.; Fedosyuk, V. M.; Kasyutich, O. I.; Schwarzacher, W. *J. Magn. Magn. Mater.* **2000**, *208*, 251.
(24) Ji, G. B.; Tang, S. L.; Gu, B. X. *J. Phys. Chem. B* **2004**, *108*, 8862.
(25) Wang, Y. W.; Zhang, L. D.; Meng, G. W.; Peng, X. S.; Jin, Y. X.; Zhang, J. *J. Phys. Chem. B* **2002**, *106*, 2502.
(26) Admon, U.; Dariel, M. P.; Grunbaum, E. *J. Appl. Phys.* **1986**, *59*, 2003.
(27) Morrish, A. H. *The Physical Principles of Magnetism*; Wiley: New York, 1965.
(28) Nguyen, A. T.; Nguyen, H. L.; Nguyen, C.; Vuong, V. H.; Nguyen, M. H. *Phys. B* **2003**, *327*, 400.
(29) Baker, B.; Pearson, R. *J. Electrochem. Soc.* **1972**, *119*, 160.
(30) Sui, T.; Yue, L.; Skomski, R.; Li, X. Z.; Zhou, J.; Sellmyer, D. J. *J. Appl. Phys.* **2003**, *93*, 10.
(31) Childress, J. R.; Chien, C. L. *J. Appl. Phys.* **1991**, *70*, 5885.
(32) Yu, M.; Liu, Y.; Sellmyer, D. J. *J. Appl. Phys.* **2000**, *87*, 9.
(33) Stoner, E. C.; Wohlfarth, E. P. *Philos. Trans. R. Soc. London, Ser. A* **1948**, *240*, 599.
(34) Skomski, R.; Coey, J. M. D. *Permanent Magnetism*; Institute of Physics: Bristol, U. K., 1999.
(35) Skomski, R.; Zeng, H.; Sellmyer, D. J. *J. Magn. Magn. Mater.* **2002**, *249*, 175.
(36) Zeng, H.; Zheng, M.; Skomski, R.; Sellmyer, D. J. *J. Appl. Phys.* **2000**, *87*, 4718.